Some limitations of surface profile reconstruction in scanning electron microscopy

ARTICLE *in* SCANNING · SEPTEMBER 2006

Impact Factor: 1.89 · DOI: 10.1002/sca.1996.4950180606

2 AUTHORS, INCLUDING:

Witold Slowko
Wroclaw University of Technology
30 PUBLICATIONS **95** CITATIONS

SEE PROFILE

SCANNING Vol. 18, 433–446 (1996)

Received August 2, 1995
Accepted with revision September 13, 1995

Some Limitations of Surface Profile Reconstruction in Scanning Electron Microscopy

T. CZEPKOWSKI AND W. SŁÓWKO

Institute of Electron Technology, Technical University of Wrocław, Wrocław, Poland

Summary: This paper is a contribution to development of electron beam profilography based on the so called "shape from shading" technique. A new formula of signal processing in a two detector system has been proposed. The formula cn be applied to all the signals showing Lambert's angular distribution. The signal processing may be realized in "real time" in a simple analog processing system. However, an accuracy of the profiles is limited by numerous errors, mainly by shadowing effects. As the shadowing causes disturbances of the signal flow, a proper design of the detection system is necessary to reduce the errors.

Key words: scanning electron microscope, secondary electron signal, topographic contrast, profile reconstruction, two-detector system

Introduction

It is a great advantage of scanning electron microscopy (SEM) that surface microtopography is displayed as brightness-modulated images (a qualitative type of contrast) in such a way that the human eye gets accustomed to see lights and shadows on macro-objects. Therefore, this technique is very convenient for searching across relatively large surface areas to find interesting details and outstanding features. That is why SEM has become one of many important testing tools in the microelectronic industry. Specialized types of SEMs are used on fabrication lines for testing so-called critical dimensions of integrated circuits and many other specific features of the structures. The disadvantage of SEM is that it gives limited quantitative information, particularly about the vertical dimensions of the surface topography.

This paper contains fragmentary results of the research project No. 8 S50100706 financed by KBN (Committee of Scientific Research) in 1994—1995.

Address for reprints:

Witold Słówko
Institute of Electron Technology
Technical University of Wrocław
ul.Janiszewskiego 11/17
50-372 Wrocław, Poland

Scientific research on surface profile reconstruction in the SEM was initiated in the 1970s (Lebiedzik 1979) and is still conducted intensively. As a result, many methods have been elaborated which generally are based on stereoscopy rules or make use of specific angular distributions of backscattered or secondary emitted electrons. In the latter case, the proposed methods consist in arranging multidetector systems for secondary or backscattered electrons and computer processing of the signals, according to many formulae and algorithms (Czepkowski 1994, Czepkowski and Słówko 1994, Hejna and Reimer 1987, Reimer *et al.* 1987, Tanaka *et al.* 1992). Theoretical considerations given to justify particular formulae of signal processing seem not quite convincing. First of all, most authors do not give enough precise consideration to the influence of the detector system geometry on a contrast formation. Thus, to obtain better accuracy, patterns for signal processing are formulated on the basis of experiments with specific SEMs, usually equipped with typical Everhart-Thornley detectors.

In this paper the problem is solved in a somewhat different way. At first, information carried by a stream of secondary electrons emitted in a defined solid angle is analyzed. As a result, the influence of the detection angles on an informative contest of the secondary electron signal is shown and a new formula for the quantitative topographic contrast is proposed. The formula seems more exact and simpler than many others applied to reconstruct surface profiles by signal processing in a two-detector system. However, there are serious limitations to the profile accuracy caused mainly by shadowing effects. The considerations may give useful suggestions about a proper design of the detector system better suited to the surface profilography. Some practical aspects connected with the adaptation of a standard SEM to the surface profiling supplement the paper.

Initial Assumptions

The signals most commonly used for surface imaging in SEMs are secondary electrons (SE) and backscattered electrons (BSE). The former kind of signal is particularly preferred for its easy detection, relatively small area, and high efficiency of generation, which make it possible to obtain images of good quality. The complex physical mechanisms of their generation have been described by many authors and are

still subjects of further investigations. In the present case, our interest mainly concerns proper methods of the signal detection in order to extract particular kinds of information, possibly in a quantitative form, and thus we can neglect the matter of the phenomena to characterize them with a few empirical expressions.

The yield of SEs generated by the primary beam (the secondary emission coefficient δ) depends on the beam incidence angle φ_p (i.e., the surface slope angle as it is shown in Fig. 1). According to Schou (1988) it can be estimated by formula:

$$\delta = \delta_0 \sec^n \varphi_p \tag{1}$$

where $n \simeq 1$ for substances with atomic number $Z \simeq 30$.

The secondary yield at $\varphi_p=0$, marked here as δ_0, depends on the energy of the primary beam and on the target material. The latter peculiarity enables one to obtain material contrast with SEs in SEM. However, there is no simple dependence between δ_0 and atomic number Z of the material. According to some authors, δ_0 depends on the ionization energy of atoms and can also be linked with the density of the material.

The most essential factor for the topographic contrast creation is an angular distribution of SE emission. For energies of the primary beam higher than that at maximum δ_0, the distribution can be approximated with good accuracy by Lambert's formula (Kanaya and Kawakatsu 1972):

$$N(\gamma) = N_0 \cos\gamma \tag{2}$$

where γ is the take-off angle of secondaries and N_0 is a number of the electrons emitted in the perpendicular direction (i.e., at $\gamma=0$). It should also be mentioned that the initial energy distribution of SEs can be characterized by two factors: the distribution half-width ΔE_h and the most probable initial energy E_p. It has been measured that ΔE_h=3–15 eV and E_p=1–5 eV for metals while insulators show much lower values. Generally, all secondaries of the initial energy < 50 eV are defined as SEs.

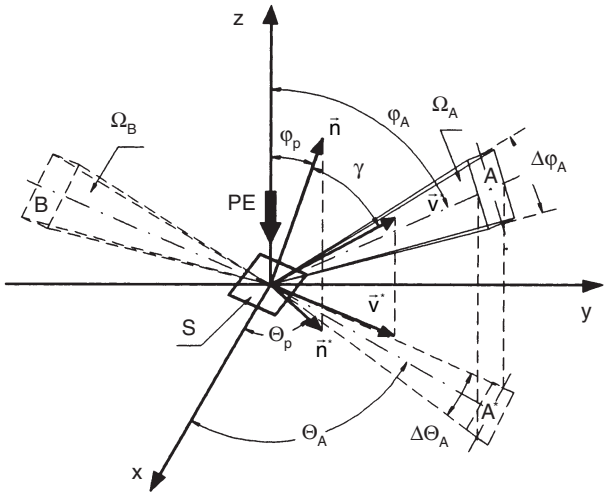

FIG. 1 Characteristic angles in a simplified detector system: A,B = detectors, PE = primary electrons, n = surface normal vector, φ_p = surface slope angle, θ_p = surface azimuth angle, φ_A = detector angle declination, γ = takeoff angle, v = initial velocity vector, $\Omega_{A,B}$ = detection solid angle.

The physical mechanism of the electron backscattering is even better understood than that of the secondary emission, but the final expressions characterizing the phenomenon are not as simple and clear as the former ones. The backscattering coefficient depends on the beam incidence angle φ_p in accordance to the empiric expression (Arnal *et al.* 1969):

$$\eta(\varphi_p) = (1+\cos\varphi_p)^{-\frac{9}{\sqrt{Z}}} \tag{3}$$

where Z is an atomic number of the target material. The coefficient shows little changes in a relatively wide range of the incidence angles φ_p (0–60°), which makes BSEs less suitable to create a good topographic contrast. The angular distribution of the BSEs is also rather complex and can be taken for a combination of the two partial patterns: (1) the Lambert's pattern for diffuse scattered electrons, and (2) a strongly directional pattern for electrons scattered in a thin surface layer and leaving the object after a few small angle collisions.

Such a shape of the angular distribution can promote a topographic contrast of the qualitative kind. However, it is rather irregular and depends strongly on the target material so that an extraction of the quantitative information about the surface topography from the BSE signal seems only slightly probable. In addition, the area of BSE generation is relatively large, and therefore the spatial resolution limit of the signal is much worse than that of SEs.

The secondaries, however, are produced not only by the impinging primary beam (usually classified as the SE1 fraction), but also by the BSEs when leaving the surface of the specimen again (called SE2). The BSEs may hit the walls of the specimen chamber of the SEM, generating there a third component of SE, the SE3. The latter fraction may be excluded from the signal by a proper design of the detector. The SE2 fraction is similar in amplitude than that of the SE1, since the backscattering coefficient η is usually of the order of 10–50% and the secondary yield is enhanced by a factor $\beta \simeq 1.5 \div 5$ for the re-emerging BSE (Hasselbach and Maier 1993, Reimer 1985). Thus, the total secondary yield δ_t can be written as:

$$\delta_t = \delta_{SE1} + \delta_{SE2} = \delta_0 \sec^n \varphi_p + \beta(\varphi_p)\cdot\eta(\varphi_p)\delta_0 \tag{4}$$

[where $\delta_{SE1}=\delta$ and is given by Eq. (1)], or in a different shape:

$$\delta_t = \delta_0 \sec^n \varphi_p [1 + f_p(\varphi_p)] = k_p \delta_0 \sec^n \varphi_p \tag{5}$$

The factor $f_p(\varphi)$ is defined as the ratio of SE2/SE1 electrons. It usually varies in the range 1–2 depending on the target material and the energy of the primary beam. Its dependence on the

beam incidence angle φ_p is rather weak and ambiguous. The ratio decreases for light materials and increases for heavy ones while φ_p is increasing. For instance, it changes from 2.2 to 1.8 for Al and from 1.3 to 1.7 for Cu when φ_p varies from 0 to 80° (Reimer and Riepenhausen 1985). The relative value of the alterations is not very great and becomes even smaller when it is referred to the coefficient k_p (greater by 1 with respect to f_p). Thus, in a first approximation it can be assumed that k_p does not depend on φ_p since an exact analytical expression has not as yet been formulated.

Detector Signals

The formation process of SE signal can be considered in a simplified detector system (Fig. 1) where one or two detectors of undefined construction (marked A and B) catch these SEs that initial velocity vectors are confined in the detection solid angle Ω_A (or Ω_B). For instance, such a detector can be imagined as an unbiased collector plate in a field-free space. According to the initial assumption mentioned above, the current of SEs coming to the detector A (or B, respectively) is given by the formula:

$$I_A = \int_{\Omega_A} i_0 \cos\gamma \sec^n \varphi_p d\Omega \tag{6}$$

and

$$i_0 = I_{PE} \frac{k_p \delta_0}{\pi} \tag{7}$$

where i_0 is the angular current density at φ_p=0, and I_{PE} is the primary electron current. The meaning of the other symbols is explained in Figure 1.

From the geometry of sphere it can be seen that

$$\begin{aligned}\cos\gamma = {} & \sin\varphi_p \cos\Theta_p \sin\varphi_v \cos\Theta_v \\ & + \sin\varphi_p \sin\Theta_p \sin\varphi_v \sin\Theta_v + \cos\varphi_p \cos\varphi_v\end{aligned} \tag{8}$$

and

$$d\Omega = \sin\varphi_v d\varphi_v d\Theta_v \tag{9}$$

The detection solid angle Ω_A results from angular dimensions of the detector which can be defined by planar angles $\Delta\varphi_A$, $\Delta\theta_A$ in polar coordinates. Thus, the integral Eq. (6) can be written in a more developed form:

$$\begin{aligned}I_A = \int_{\varphi_{A1}}^{\varphi_{A2}} \int_{\Theta_{A1}}^{\Theta_{A2}} & i_0 \sec^n \varphi_p \left[\sin\varphi_p \cos\Theta_p \sin\varphi_v \cos\Theta_v \right. \\ & \left. + \sin\varphi_p \sin\Theta_p \sin\varphi_v \sin\Theta_v + \cos\varphi_p \cos\varphi_v \right] \sin\varphi_v d\varphi_v d\Theta_v\end{aligned} \tag{10}$$

where bounds of the integral are defined as:

$$\begin{aligned}\varphi_{A1} &= \varphi_A - \frac{\Delta\varphi_A}{2} \quad , \quad \varphi_{A2} = \varphi_A + \frac{\Delta\varphi_A}{2} \\ \Theta_{A1} &= \Theta_A - \frac{\Delta\Theta_A}{2} \quad , \quad \Theta_{A2} = \Theta_A + \frac{\Delta\Theta_A}{2}\end{aligned} \tag{11}$$

After integration it takes the following form:

$$\begin{aligned}I_A = i_0 \sec^n \varphi_p \Bigg\{ & \sin\varphi_p \cos\Theta_p \left[\frac{1}{2}(\varphi_{A2} - \varphi_{A1}) - \frac{1}{4}(\sin 2\varphi_{A2} \right. \\ & \left. - \sin 2\varphi_{A1}) \right] (\sin\Theta_{A2} - \sin\Theta_{A1}) - \sin\varphi_p \sin\Theta_p \\ & \left[\frac{1}{2}(\varphi_{A2} - \varphi_{A1}) - \frac{1}{4}(\sin 2\varphi_{A2} - \sin 2\varphi_{A1}) \right] (\cos\Theta_{A2} \\ & - \cos\Theta_{A1}) + \frac{1}{2}\cos\varphi_p (\sin^2\varphi_{A2} - \sin^2\varphi_{A1})(\Theta_{A2} - \Theta_{A1}) \Bigg\}\end{aligned} \tag{12}$$

After a series of transformations, this complex expression can be brought to a clearer form:

$$I_A = I_{PE} \frac{\delta_0 k_p}{\pi} \sec^n \varphi_p \left[d_A \sin\varphi_p \cos(\Theta_A - \Theta_p) + c_A \cos\varphi_p \right] . \tag{13}$$

where c_A and d_A are coefficients depending on geometrical dimensions and position of the detector. The coefficients are defined by the following expressions:

$$\begin{aligned}c_A &= 2\Delta\Theta_A \sin\varphi_A \sin\frac{\Delta\varphi_A}{2} \cos\varphi_A \cos\frac{\Delta\varphi_A}{2} \\ &= \Omega_A \cos\varphi_A \cos\frac{\Delta\varphi_A}{2}\end{aligned} \tag{14}$$

$$d_A = (\Delta\varphi_A - \cos 2\varphi_A \sin\Delta\varphi_A) \sin\frac{\Delta\Theta_A}{2} \tag{15}$$

The above formula for the detector current undergoes further simplification when the detector is placed in the xz plane (θ_A=0) and n=1 (true for elements with atomic number close to 30):

$$I_A = I_{PE} \frac{\delta_0 k_p}{\pi} (d_A tg\varphi_p \cos\Theta_p + c_A) \tag{16}$$

Resulting from the above expression, the detector signal depends on the azimuth angle θ_p and the slope angle φ_p of the target surface which implies a topographic contrast. It also depends on a local value of the secondary emission coefficient

Δ_0 which is a source of the material contrast. Both kinds of contrast cannot be fully separated for the signal of the single detector. However, it is possible to enhance one kind of contrast, suppressing to some extent the second kind by appropriate changes in geometry of the detector. This is achieved by means of the coefficients d_A and c_A which can be called, respectively, the topographic contrast coefficient and the material contrast coefficient.

The dependence of the coefficients (and their ratio d_A/c_A) upon the detector declination angle φ_A at various solid and vertical angles of detection Ω_A, $\Delta\varphi_A$ is shown in the Figure 2a,b, and c. It should be noticed here that maximum values of the coefficients increase proportionally to the detection solid angle Ω_A. However the material contrast coefficient c_A attains its maximum at the detector declination angles φ_A close to zero, while the topographic contrast coefficient d_A is greatest for $\varphi_A \simeq \pi/2$. Influence of the vertical detection angle $\Delta\varphi_A$ is less considerable, but its lower values seem better for the material contrast.

The above conclusions are consistent with the results of the experiments described by numerous authors (e.g., Hejna 1994), which makes the presented model more reliable.

Topographic Contrast in a Two-Detector System

A method for the separation of the topographic and material contrast was initially proposed for the BSE signal by Suganuma in 1963 and applied by Kimoto *et al.* (1966). The authors made use of two semiconductor detectors placed symmetrically on the face of the objective lens. They got substantial enhancement of the topographic contrast by substraction of the detector signals and almost pure material contrast by their addition.

Similar effects can be attained in a system of two SE detectors. When the two detectors (marked A and B in Fig. 1) are quite identical and placed symmetrically (i.e., $\theta_B=\theta_A+180^\circ$), the expression (13) for the current of the detector B takes the following form:

$$I_B = I_{PE}\frac{\delta_0 k_p}{\pi}\sec^n\varphi_p\left[c_B\cos\varphi_p - d_B\sin\varphi_p\cos(\Theta_A-\Theta_p)\right] \tag{17}$$

Symmetry of the detector system also implies that:

$$d_A = d_B = d^* \quad , \quad c_A = c_B = c^* \tag{18}$$

Then, addition and substraction of the both signals gives the following results:

$$I_A + I_B = I_{PE}\frac{\delta_0 k_p}{\pi}2c^*\sec^{n-1}\varphi_p \tag{19}$$

and

$$I_A - I_B = I_{PE}\frac{\delta_0 k_p}{\pi}2d^*\sec^{n-1}\varphi_p tg\varphi_p\cos(\Theta_A-\Theta_p) \tag{20}$$

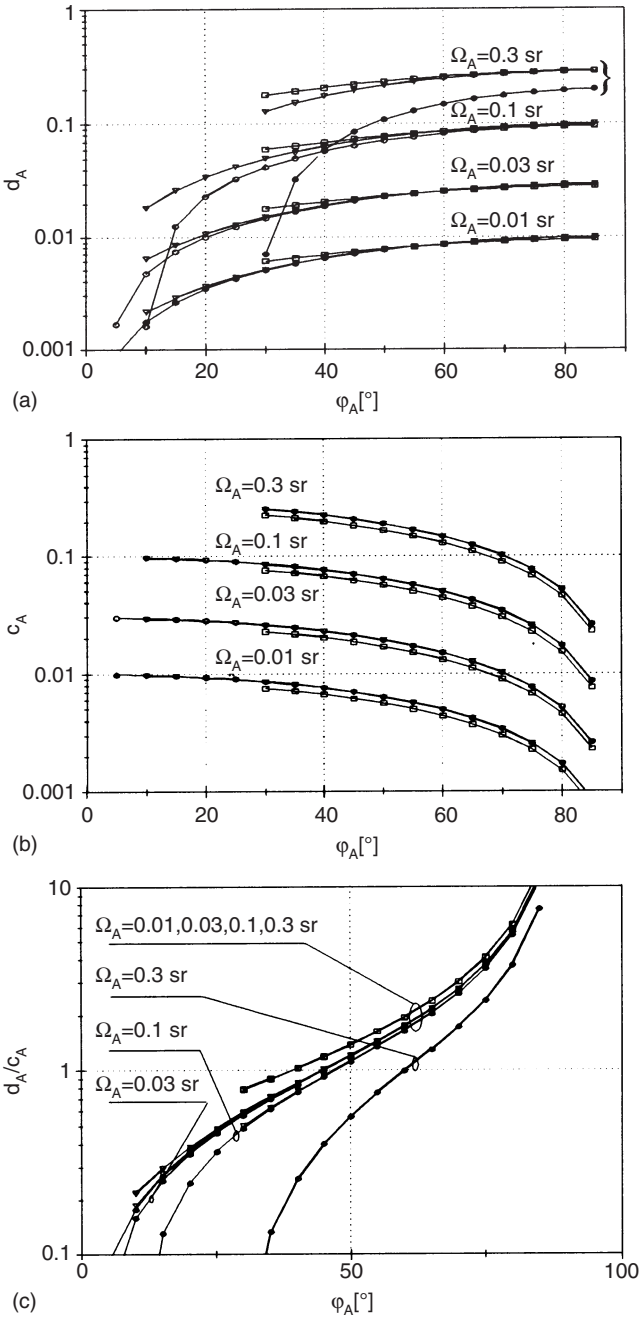

FIG. 2 Influence of the detector declination angle on (a) the topographic contrast coefficient, (b) the material contrast coefficient (c) ratio of both coefficients, (for various detection solid angles Ω_A and vertical detection angles $\Delta\varphi_A$= –0.1 rad, –▽– = 0.3 rad, –□– = 1.0 rad).

Thus, according to the earlier expectations, the sum of detector signals shows mostly material contrast connected with alterations of the SE coefficient δ_0. The influence of the surface slope angle φ_p (connected with topography) can be neglected because $n \simeq 1$ for most materials and k_p depends on φ_p relatively weakly. However, the subtraction of the signals still gives mixed contrast. Its full differential (for n=1, θ_p=const., k_p=const.)

$$d(I_A - I_B) = 2d^* \frac{I_{PE} k_p}{\pi} \cos(\Theta_A - \Theta_p) \left(tg\varphi_p d\delta_0 + \frac{\delta_0 d\varphi_p}{\cos^2 \varphi_p} \right) \tag{21}$$

can be considered an alternate component of the signal, and its parts in brackets represent the material and the topographic modulation, respectively. As the material modulation disappears at φ_p=0, the topographic contrast can be separated only for small slope angles of the surface. However, it is easy to notice that the material contrast can be fully eliminated by division of the difference signal by the summary signal which leads to the following expression:

$$\frac{I_A - I_B}{I_A + I_B} = \frac{d^*}{c^*} tg\varphi_p \cos(\Theta_A + \Theta_p) \tag{22}$$

It should be noted that all the factors, such as k_p or $\sec^n \varphi_p$ known only poorly, disappear in this final version. Thus, the final conclusion arises that quantitative topographic contrast defined by the above expression originates exclusively from the Lambert angular distribution of the emission current density. That means that the formula discussed can also be applied to other signals liable to the Lambert's law.

The first who proposed this manner to separate the topographic contrast were Reimer *et al.* (1987), but the final formula derived by them had a somewhat different shape. According to them, the above quotient was proportional to $\sin\varphi_p$ (instead to $tg\varphi_p$). The difference has not only a formal meaning but some practical implications as well. When both detectors are placed in the xz plane (i.e., θ_A=0), the expression (22) takes the following shape in rectangular coordinates:

$$\frac{I_A - I_B}{I_A + I_B} = \frac{d^*}{c^*} \frac{dz}{dx} \tag{23}$$

Thus, an integral of the expression represents the profile of the surface along x axis, i.e.,:

$$\int \frac{I_A - I_B}{I_A + I_B} \frac{c^*}{d^*} dx = z(x) \tag{24}$$

The above formula is relatively simple and can be realized not only by computer processing of the signals, but also in a proper analog processing system. The latter solution seems very convenient because the profile imaging may be realized immediately (in real time) on a SEM monitor working in the Y-modulation mode. Besides, the image reacts immediately to all the manipulations of the operator. If a magnification of the image is the same in perpendicular (z) and lateral (x) directions, the height and the slope of the surface forms can be read out directly on the monitor screen with a measuring graticule.

Shadowing Effect

Analyzing the formulae presented above one should remember that the range of their functioning is physically limited. The main limitation results from the fact that initial velocities of the emitted electrons can be tangent to the sample surface at the most ($\gamma \leq 90^\circ$). Thus, the expression Eq. (16) for the detector current cannot become negative. In the case of a point detector ($\Delta\varphi_A \to 0$), the conditions can be formulated as:

$$\frac{d_A}{c_A} tg\varphi_p \leq 1 \tag{25}$$

That means c_A/d_A is the maximum value of $tg\varphi_p$, for which the detector is still over the plane tangent to the sample surface in the impingement point and is able to collect SEs. Besides this elementary kind of shadowing, which may be called the shadowing by the tangent plane, elements of the surface topography can also shadow the detector. In practice the problem becomes more complicated because dimensions of the detector are always finite, and furthermore it may be partly shadowed to various extents. Thus, the expression (16) for the detector current will have to be modified according to the kind and extent of the shadowing and even according to the shape of the shadowing topographic elements.

It is quite obvious that there are shadowing effects that contribute significantly to the final error of the profile reconstruction. The problem can be considered most generally in the case of shadowing by the tangent plane shown in Figure 3. Since the SEs are able to move only over the plane, they cannot reach the shadowed part of the detector situated beneath. To evaluate a current of the detector in this case, the expression Eq. (10) should be integrated into new bounds depending on the inclination and azimuth angles of the normal to the plane (φ_p, θ_p). A boundary of the shadow is determined by the line of intersection of the detector and the plane. Using Neper formulae for the spherical triangle shown in Figure 3. we can get the equation:

$$\begin{aligned} \cos\ 90^\circ = &\cos\varphi^*_{A2} \cos\varphi_p \\ &+ \sin\varphi^*_{A2} \sin\varphi_p \cos(-\Theta_p + \Theta_A) \end{aligned} \tag{26}$$

and after proper transformations the following expression for the upper boundary angle of the shadowed detector:

$$\varphi^*_{A2} = \operatorname{arc} tg\left[\frac{-ctg\varphi_p}{\cos(\Theta^*_A - \Theta_p)}\right] \tag{27}$$

where θ_A^* is a current value of the azimuth angle within the detector ($\theta_{A1} \le \theta_A^* \le \theta_{A2}$). An analogous expression determines the shadow boundary for the detector B.

To evaluate a current collected by each detector, the expression (10) should be integrated numerically within its unshaded surface. In turn, this makes it possible to estimate errors of the profile reconstruction caused by the shadowing effect. The most objective measure of the disturbances seems to be a relative error of the profile slope defined as:

$$\frac{\Delta z'}{z'} = \frac{S_z - S_I}{S_I} \tag{28}$$

where S_I is an ideal quantitative topographic contrast and S_z is its disturbed value, according to the expressions:

$$\frac{d^*}{c^*} tg\varphi_p \cos(\Theta_A - \Theta_p) = S_I \tag{29}$$

and

$$\frac{I^*_A - I^*_B}{I^*_A + I^*_B} = S_z \tag{30}$$

I_A^* and I_B^* are detector currents calculated from Eq. (10) in the shadowing conditions.

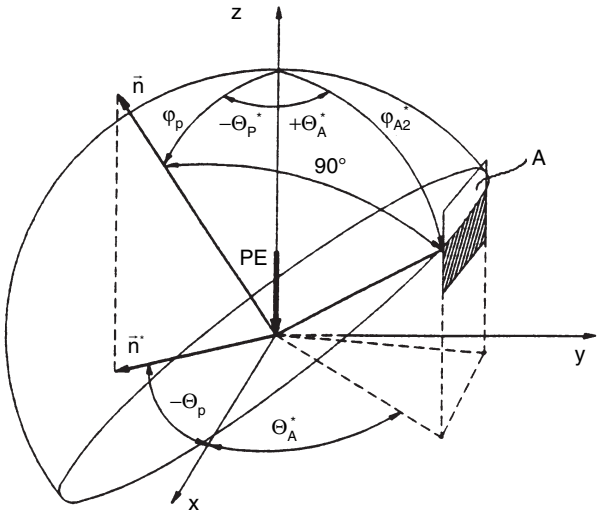

FIG. 3 Shadowing by the tangent plane.

On the basis of the above-mentioned expressions, a set of computations has been conducted. For instance, some results have been shown in Figure 4 in a form of diagrams illustrating the dependence of the relative slope error $\Delta z'/z'$ upon the surface inclination angle θ_p, for a few variants of the detector geometry (the same as in Fig. 2) and two azimuth angles θ_p. In the diagrams, the beginning and the moment when the detector is fully shadowed have been marked by letters S and E, respectively.

Conclusions derived from Figure 4 are quite similar to those expected from Figure 2. As it was mentioned, the quotient d^*/c^* defines the maximum surface slope angle φ_p for which the detector still remains unshaded. Thus, in order to minimize the shadowing errors, a possibly small value of the quotient should be ensured by reduction of the detector declination angle $\varphi_{A,B}$. The vertical detection angle $\Delta\varphi_{A,B}$ should also be small, but its influence is less considerable. The diagrams in Figure 4 concern only one value of the detection solid angle $\Omega_{A,B}$ (and the detection horizontal angle associated with the latter at fixed $\Delta\varphi_{A,B}$), because its increase does not cause

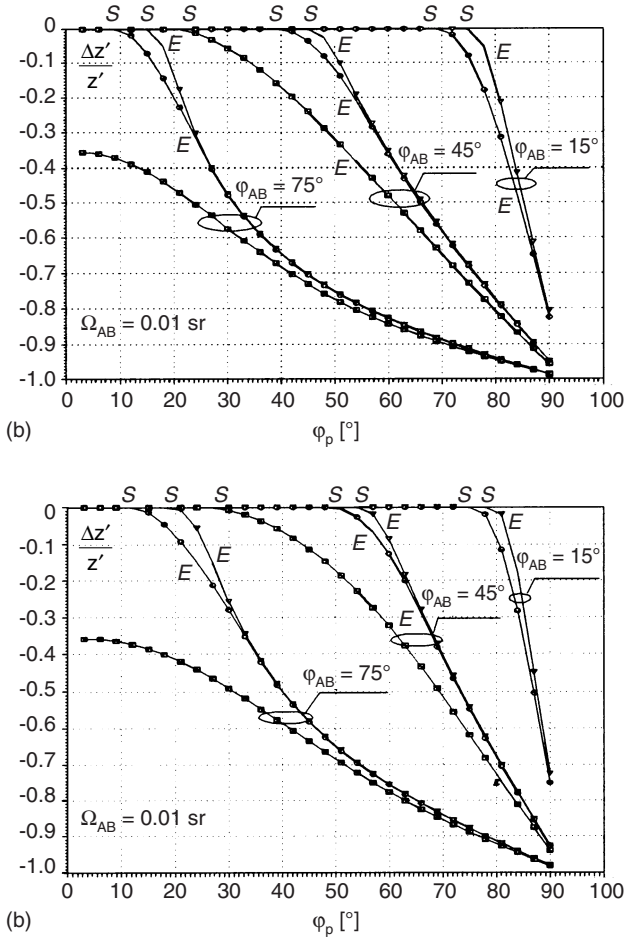

FIG. 4 Relative error of the profile slope caused by the shadowing effect as a function of the surface slope angle φ_p for three values of the vertical detection angle $\varphi_{A,B}$ (▽ = 0.1 rad, ○ = 0.3 rad, □ = 1.0 rad) and two values of the surface azimuth angle θ_p: (a) θ_p=0, (b) θ_p=45° (θ_A=0, θ_B=180°, S = shadowing begins, E = full shadowing).

any distinct disturbances of the profiles. It may even be profitable for a stronger signal and less noise. Also, an increase of the azimuth angle results in a smaller shadowing error which can be seen in Figure 4b. Finally, we can conclude that it is possible to get an undisturbed profile up to its slope angle $\varphi_p \simeq 75^\circ$, when the detectors are placed at a reasonable declination angle $\varphi_{A,B} \simeq 15^\circ$ and show a small detection angle $\Delta\varphi_{A,B}$.

The profile slope error in the next stage, that is, after integration of Eq. (24), results in a wrong shape of the profile reconstructed. This error depends on a sequence of the local slopes, that is, on the real shape of the surface. The profile that seems most convenient for testing of the shadowing errors is a semicircular profile, because it presents a full variety of the slope (incidence) angles from 0 to 90°. As an example, results of the computations made for the same detector geometry as in Figure 4 have been shown in Figure 5. From the diagrams drawn in a normalized coordinates, it follows that disturbances of the semicircular profile arise at its beginning where slope angles are high. In this part the profile is reconstructed in the shape of a straight line instead an arc. Its inclination and length depends mainly on the detector declination angle $\varphi_{A,B}$. The relative error connected with the deformations may be defined as:

$$\frac{\Delta z(x)}{z_0(x)} = \frac{z_0(x) - z(x)}{z_0(x)} \tag{31}$$

where z(x) is the height of the reconstructed profile at a given point x and $z_0(x)$ is the height of the perfect profile (arc) at this point. The error starts with 100% at the beginning (for $\varphi_p = 90^\circ$), then drops and stabilizes its value in the top part. The minimal error in the conditions is about 18% (for $\varphi_{A,B} = 15^\circ$), not too small an error at that point. The error can be reduced by increasing the output signal amplificationto such an extent that a proper height of the profile can be achieved. The case corresponds to diagrams shown in Figure 5b. However, the way of system calibration cannot fully eliminate the shape of the error at the profile sides, and its relative value may by defined as:

$$\Delta^* z(x) = \frac{\left[\frac{z_0(x)}{r} - \frac{z(x)}{z_{\max}}\right]}{\frac{z_0(x)}{r}} = 1 - \frac{z(x) r}{z_{\max} z_0(x)} \tag{32}$$

where r is the radius of the circle, that is, the height of the ideal profile, and $z_{\max}$ is the height of the reconstructed profile. In this case, the local value of the error drops from 100% to 0 with a gradient depending on the detector declination angles $\varphi_{A,B}$.

It should be also noticed here that the semicircular profile is a very severe test for the detection system because its inclination angles φ_p exceed 60° within a half of its height. Profiles of less steep slopes could be reconstructed almost perfectly in the detector system geometries examined here.

Influence of the Extracting Field on the Boundary Detection Angles

Commercial SEMs are usually equipped with Everhart-Thornley scintillator detectors. Their focusing electrodes are biased with a positive voltage (the extracting voltage) attracting SEs to entrance windows of the detectors. In this case, both

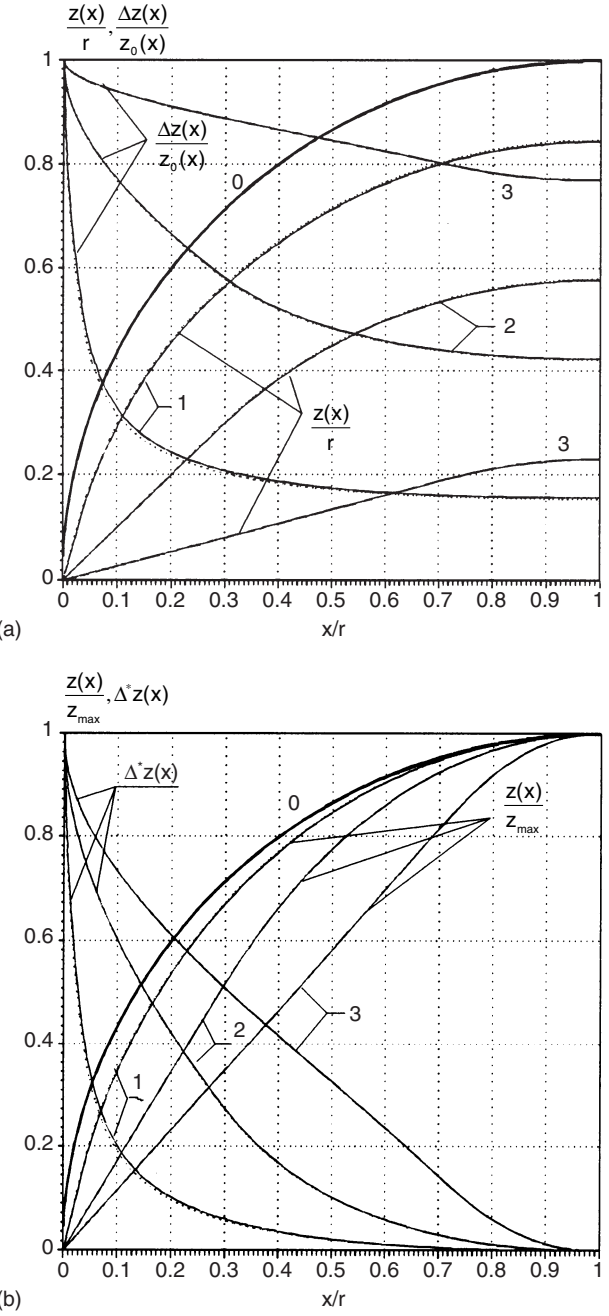

FIG. 5 Semicircular profile of the surface and its deformations caused by shadowing for three values of the detector declination angle (curves: 0—perfect shape, 1—$\varphi_{A,B}=15^\circ$, 2—$\varphi_{A,B}=45^\circ$, 3—$\varphi_{A,B}=75^\circ$, $\Delta\varphi_{A,B}=5.7^\circ$, $\theta_A=0$, $\theta_B=180^\circ$, $\theta_p=0$, $\Omega_{A,B}=0.01$ srad), (a) profiles referred to radius of the semicircle r and their relative errors, (b) profiles referred to their maximum height $z_{\max}$ and their relative errors according to Eq. (32).

the detector current and the signal-to-noise ratio increase, but electron trajectories are no longer straight lines and the detection angles cannot be evaluated simply from geometrical dimensions of the detector system. However, E-T detectors as a rule are so large that they have to be placed far away from the sample stage and their declination angle $\varphi_{A,B}$ in no extracting field space would be too large (about 90°) to obtain any decent profile. It would be interesting then whether or not the extracting field can improve the situation essentially. The extracting-field distribution and electron-optical properties of the field depend directly on a given design of the detector system and the sample chamber. Thus, it should be investigated individually on a specific example. An object of the present considerations was our SEM (of our own design, Drzazga *et al.* 1987) called the MR-11. For the two detector systems used in this microscope, a series of computations has been made to establish their characteristic detection angles for various variants of the polarizing potential and the stage position. To obtain necessary data about field distributions and SE trajectories, a package of computer programs called "Optel-Asym" has been applied. An example of the extracting-field distribution in the sample chamber is shown in Figure 6.

The distribution demonstrates symmetry with respect to the yz plane, and thus it will be possible to analyze electron trajectories only on one side of it. It is noticeable that the intensity of the extracting field is rather low, particularly at the beam axis where a characteristic potential saddle is formed. It suggests that the field can influence substantially only the electrons of relatively low initial energies. As a consequence, the characteristic detection angles, defined by the directions of initial velocities accepted by the detector, must depend strongly on the initial energies. The detection angles certainly depend also on the sample stage position, as the examples in Figure 7 illustrate it.

Thus, to get necessary information about characteristic parameters of the detector system, it is necessary to make computations for very numerous variants of the initial conditions. Some partial results of the computations have been shown in Figure 8. The diagrams illustrate a depe. The diagrams illustrate a dependence of the vertical and the horizontal detection angles as well as the detector declination angle on the initial energy of SEs for two positions of the sample stage. As electron trajectories for the initial energy E_{SE}=100eV and the extracting potential U_e=50V are almost straight lines, the detection angles computed for this energy can be considered to be close to those defined in no extracting field case. We can, therefore, conclude finally that the characteristic parameters of the detector system cannot be improved essentially by the extracting field, though it reduces slightly the detector

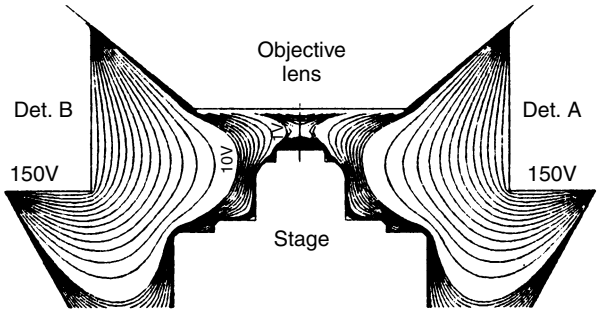

FIG. 6 Plot of the equipotential lines corresponding to the extracting field in the sample chamber of MR-11 (working distance H=10 mm).

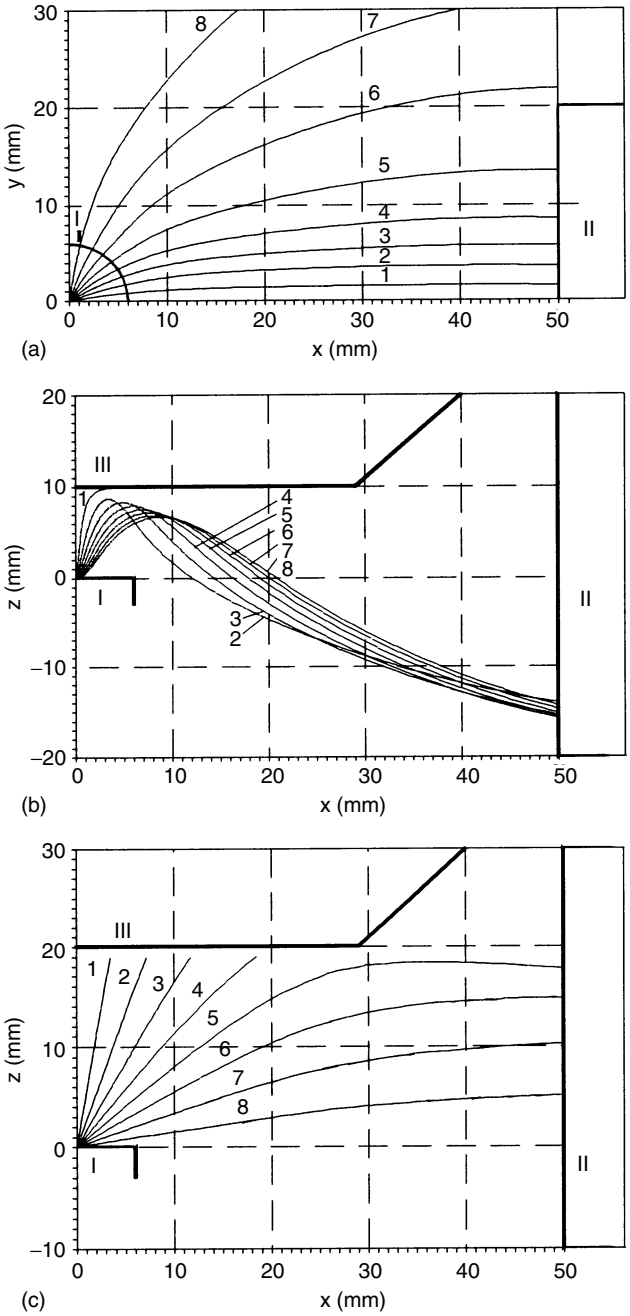

FIG. 7 Electron trajectories in the sample chamber of MR-11 (I = stage, II = detector, III = objective lens, extracting voltage U_e=150 V, inclination angles or azimuth angles of initial velocities, φ_v or θ_v respectively: 1 = 10°, 2 = 20°, ..., 8 = 80°): (a) trajectories in xy plane for initial energy E_{SE}=0.1 eV, working distance H=10 mm; (b) trajectories in xz plane in the same conditions as in (a); (c) trajectories in xz plane for E_{SE}=12.5 eV, H=20 mm.

declination angle $\varphi_{A,B}$ but increases the vertical detection angle $\Delta\varphi_{A,B}$ at the same time. As a result, the detector parameters seems quite unsuitable for the profiles reconstruction. Data readout at the most probable initial energy ($\varphi_{A,B}\simeq 60^\circ$, $\Delta\varphi_{A,B}\simeq 50^\circ$, $\Delta\theta_{A,B}\simeq 70^\circ$ for $E_{ESp}\simeq 2$eV) compared with those in Figure 4 indicate that profiles reconstructed in the detector system will be disturbed by the shadowing effect for the surface inclination angles φ_p greater than 25°. Thus, a solution for the problem should rather be sought in a new design of the detector system that would be better fitted to the specific task.

Distortion of the Profiles

As mentioned before, the extracting field is disposed symmetrically at both sides of the optical axis where it forms a potential saddle. Thus, the division of SEs between the two detectors depends not only on the direction of their initial velocities but also on the place of their generation involving a direction of the extracting forces. An illustration of the mechanism is seen in Figure 9. where trajectories of electrons emitted from two points lying on the two opposite sides of the optical axis are shown. It is easy to notice that all electrons with the initial velocities inclined toward the right detector reach the target when they are emitted from the point placed at the same side of the stage. However, only half the number of the electrons can hit the detector when they are emitted at the opposite side. It has been established experimentally that the dependence between the detector signal and the x coordinate of the emission point can be considered linear (for small x and a flat surface) as beneath:

$$I_{A,B}(x) = I_0 \pm kx \tag{33}$$

where I_0 is a signal at the optical axis and k is a proportionality factor. Thus, the integral Eq. (24) can be written in the following form:

$$z_d(x) = \frac{c^*}{d^*}\int \frac{I_A - I_B}{I_A + I_B}dx = k_0\frac{x^2}{2} \tag{34}$$

where $k_0 = kc^*/I_0d^*$.

The parabolic deformation of the flat profile can be partly compensated by a negative voltage (−c) added to the processed signal:

$$z_d(x) = \frac{c^*}{d^*}\int\left(\frac{I_A - I_B}{I_A + I_B} - c\right)dx = k_0\frac{x^2}{2} - cx \tag{35}$$

In this case, the maximal distortion error arises at half the line length x_k, so it is four times less than its uncompensated value, namely:

$$z_{dm} = z\left(\frac{x_k}{2}\right) = -k_0\frac{x_k^2}{8} \tag{36}$$

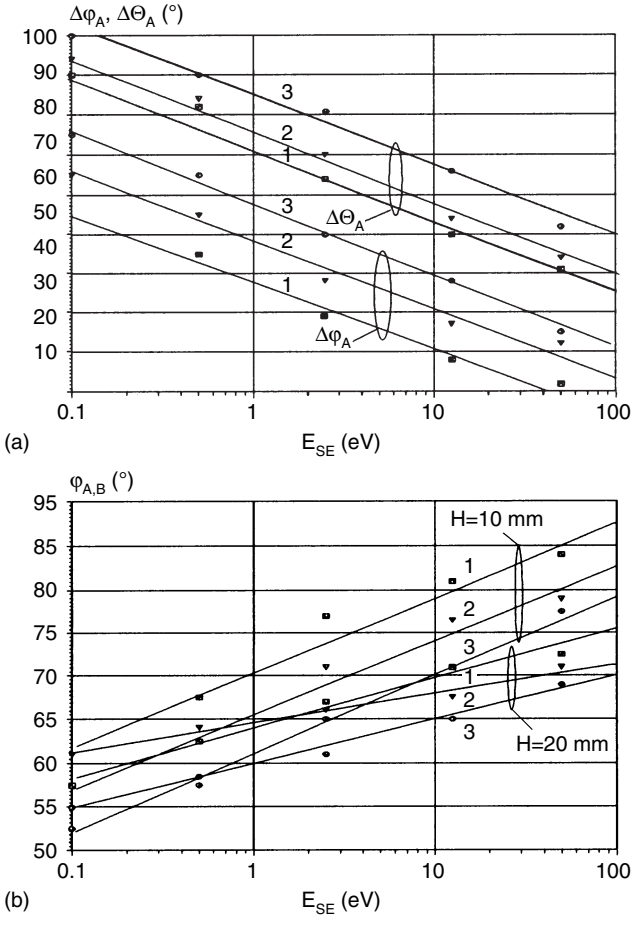

FIG. 8 Characteristic angles of the detector system in MR-11 versus the initial energy of secondary electrons (the extracting voltage U_e: 1 = 50 V, 2 = 150 V, 3 = 450 V): (a) horizontal and vertical detection angle $\Delta\theta_A$, $\Delta\varphi_A$ for working distance H=10 mm, (b) detector declination angle φ_A for two working distances H=10 mm and H=20 mm.

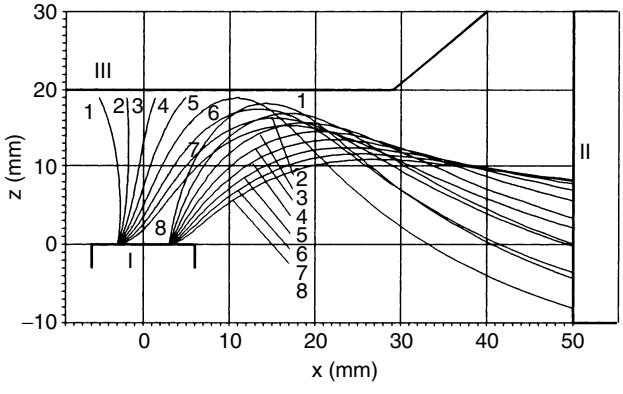

FIG. 9 Trajectories of secondary electrons emitted from two points placed symmetrically at a distance of 3 mm from the electron-optical axis (I = stage, II = detector, III = objective lens, initial energy E_{SE}=0.5 eV, extracting voltage U_e=150 eV, working distance H=20 mm, inclination angles of initial velocities φ_v, respectively: 1 = 10°, 2 = 20°, ..., 8 = 80°).

An instance of the profile distortion observed in the microscope MR-11 is shown in Figure 10. As the line lengths on the sample surface and the monitor screen are tied by the image magnification M, the relative distortion error is inversely proportional to the magnification, that is,:

$$\frac{z_{dm}}{z_p} \sim \frac{1}{M} \tag{37}$$

where z_p is the height of the profile. In the case of MR-11, the error can be neglected for magnifications greater than a few hundred, that is, for the scan line length < 0.1 mm; so the distortion error may create any real problems only when relatively big objects are examined.

Some Experimental Results

As mentioned earlier, the detection system of the MR-11 microscope is rather improper for the surface profile reconstruction when the sample demonstrates a more developed topography. Large values of the declination and detection angles $\varphi_{A,B}$, $\theta_{A,B}$ result in relatively high d^*/c^* ratios (between 2 and 4), which means that the topographic contrast will attain saturation at low values of the surface slope angle φ_p. However, an arrangement based on the microscope could be useful for the profilometry of smooth objects and might give the experience necessary to design a new improved system. The main part of the arrangements should be a proper signal processing system capable to make a set of mathematical operations on signals of both detectors according to the formula (24). Thus, a computer system has been elaborated which enables to record both signals simultaneously on a hard disc and process them according to any optional algorithm.

As an example of the function of the system, the detector signals at successive stages of the processing are shown in Figure 11. An object of the profiling was a ball of the radius r=0.5 mm impressed in copper to the depth h=11 μm (a diameter of the print is ∅0.2 mm).

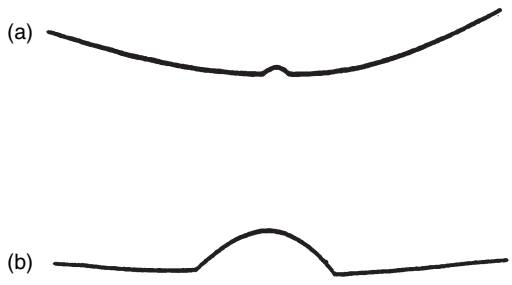

FIG. 10 Profile distortion observed in the microscope MR-11 (after partial compensation): (a) shape at the magnification M=6, (b) shape at the magnification M=40.

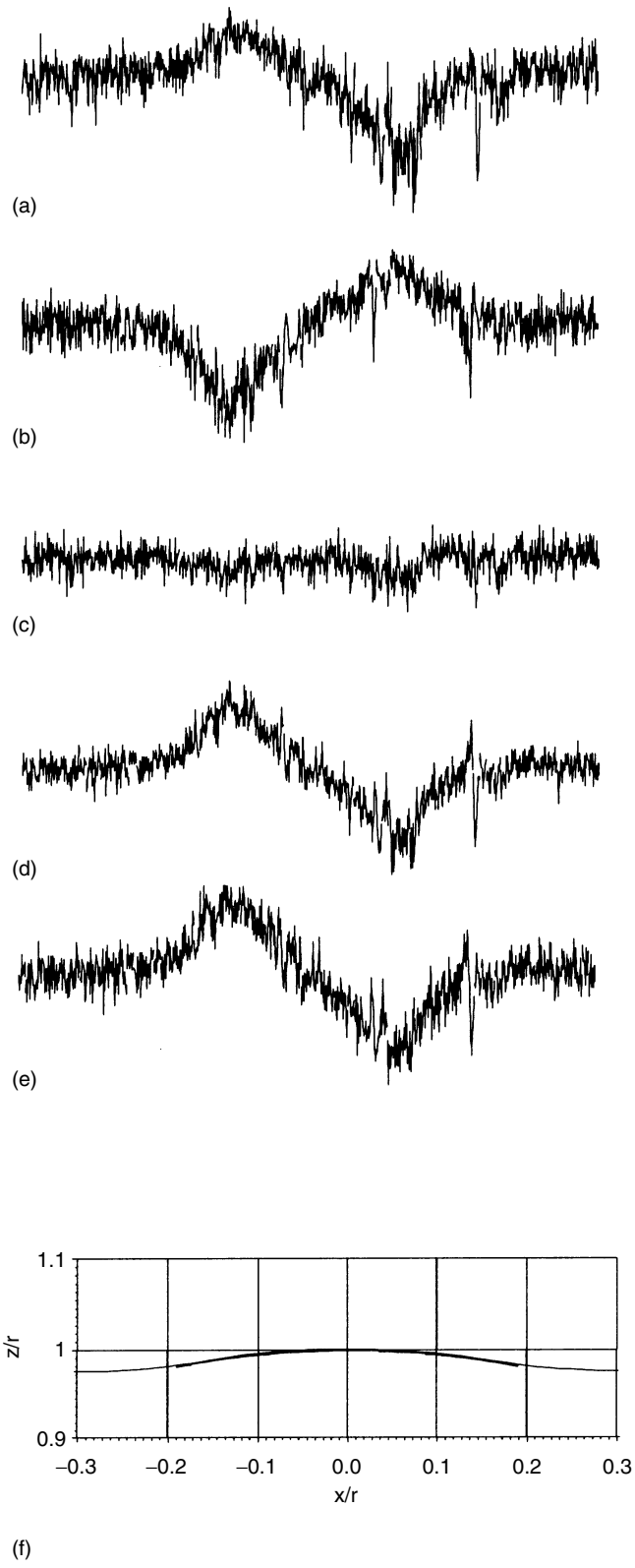

FIG. 11 Detector signals at successive stages of the processing (for ball print in copper of radius r=0.5 mm, sag h=11 μm, i.e., r/h=45.5): (a) I_A, (b) I_B, (c) I_A+I_B, (d) I_A-I_B, (e) $(I_A-I_B)/(I_A+I_B)$, (f) profile reconstructed according to Eq. (24).

In so small a depression, the surface inclination angles nowhere exceed 11°. Thus, a relatively high sensitivity of the system to the topographic contrast does not imply shadowing errors in this case. The reconstructed profile (Fig. 11f) fits almost perfectly to an exactly circular shape (heavy line). This is even a bit surprising, because a weakly modulated signal seems very noisy.

It is also noticeable that the signal profiles are almost straight lines because $\sin\varphi_p$, $\mathrm{tg}\varphi_p$, and many other functions are nearly linear for small arguments. That is probably why Tanaka *et al.* (1992) have achieved a good accuracy of the surface profiles obtained for relatively smooth objects (rigid disks) using a bit different formula of the signal processing.

In turn, the shape of signals at successive stages of the processing is also shown in Figure 12, but this time the depth of the ball print was much greater (h=0.164 mm, r/h=1.52) as was the maximum inclination angle ($\varphi_p \leq 70°$). Thus, symptoms of shadowing errors can be easily noticed. First of all, the sum of signals (Fig. 12c) no longer is constant, that is, independent of the surface slope, and resembles the shape of input signals at its sides. Besides, the final profiles in Figure 12f demonstrate too low a height and sides that are not quite circular. For comparison, the theoretical shape of the signals computed in not shadowing and shadowing conditions is shown in Figure 13.

Computer systems are very convenient for experiments with signal processing according to various formulae which can be conducted perfectly on the same input signals. However, our computer system for signal processing has been arranged on the basis of PC486DX, so it is not powerful enough to process signals in a "real time." This is a serious disadvantage in an experimental work, where an observed image should react immediately to all manipulations of the SEM operator.

For general purposes, an analog processing system seems more convenient. A circuit diagram of the analog system applied in MR-11 is shown in Figure 14. The system was built on precise integrated circuits OPA27 and MPY634 (Burr-Brown). Signals of both detectors are lead to inputs A and B for subtraction and addition (circuits U2 and U1). The operations of division and integration are realized by the successive circuit U3 and U4. The result of the integration is zeroed at the start of each line by line suppression pulses PS. Signals at each processing stage can be chosen by the changeover switch P5 to be observed on the monitor. A proper amplification of the system, that is, its proper calibration, can be fixed with the potentiometer R42 at the input of the final amplifier.

Some examples of the images and profiles obtained in the system are shown in Figure 15. The object shown in Figure 15a,b is a ball 0.5 mm in diameter pressed at 0.15 mm in copper. This time, the sides of the print are very steep and shadowing errors cannot be neglected. However, their presence is not distinctly seen there, because a calibration of the system has been conducted just on that object. Thus, the height of the profile is correct while the shape of its sides can be slightly disturbed. The same concerns profiles in Figure 15d, which imagine etching in silicon. In this case, the object is an eleva-

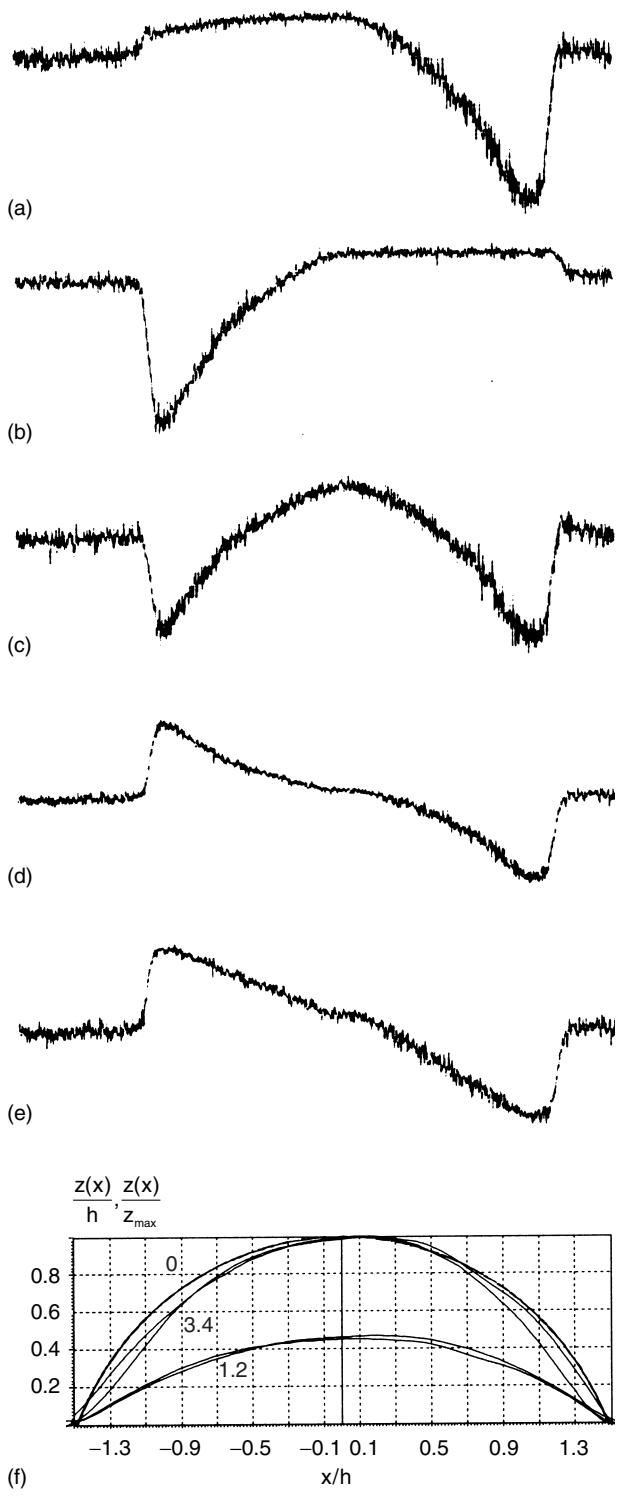

FIG. 12 Detector signals at successive stages of the processing (for ball print in copper of radius r=0.25 mm and sag h=0.164 m, i.e., r/h=1.25): (a) I_A, (b) I_B, (c) I_A+I_B, (d) I_A-I_B, (e) $(I_A-I_B)/(I_A+I_B)$, (f) profile reconstructed in two different scans (0 = perfect profile; 1,2 = z(x)/h, profiles obtained after proper calibration on the object in Fig. 10; 3,4 = $z(x)/z_{max}$, profiles related to their disturbed maximum height).

tion while the profiles are directed down the picture because of the reverse order of signal subtraction.

The mentioned correction of shadowing effects is possible only in the rare case when the right height of a profile is known, which makes it not very useful. A more general solution of the problem should be sought in a new detector system of proper detection angles to reduce shadowing.

The next serious source of the profile errors can be the charging effects. Since the method is based on the angular distribution of SE emission, any electric fields that affect trajectories of SEs may spoil the right shape of profiles. An influence of the sample charging can also be observed in Figure 15c, where charged dust particles on the top and the side of the object produce dark and light stripes in the micrograph. The particles can also be seen on the profiles in Figure 15d. However, their electric charges introduce an asymmetry to the signal detection which results in a displacement of the profiles or even leads to their intersecting. As a remedy for charging effects, a low-energy electron beam can be applied. It should work in the beam energy range of 0.5 keV to 2 keV, where $\delta \geq 1$ is attainable for most dielectric materials.

The application of the low-energy electron beam may also

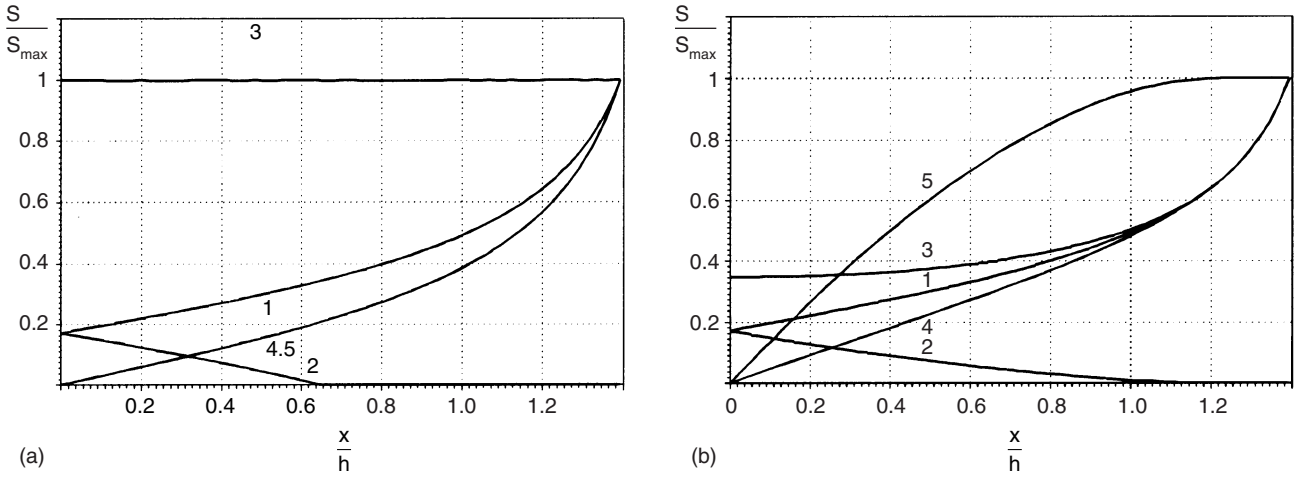

FIG. 13 Theoretical shape of the detector signals at successive stages of processing computed according to Eqs. (12) and (27) for the object in Figure 12 and the detection angles as in MR-11: (a) without shadowing, (b) with shadowing (r/h=1.52, 1—$S=I_A$, 2—$S=I_B$, 3—$S=I_A+I_B$, 4—$S=I_A-I_B$, 5—$S=(I_A-I_B)/(I_A+I_B)$.

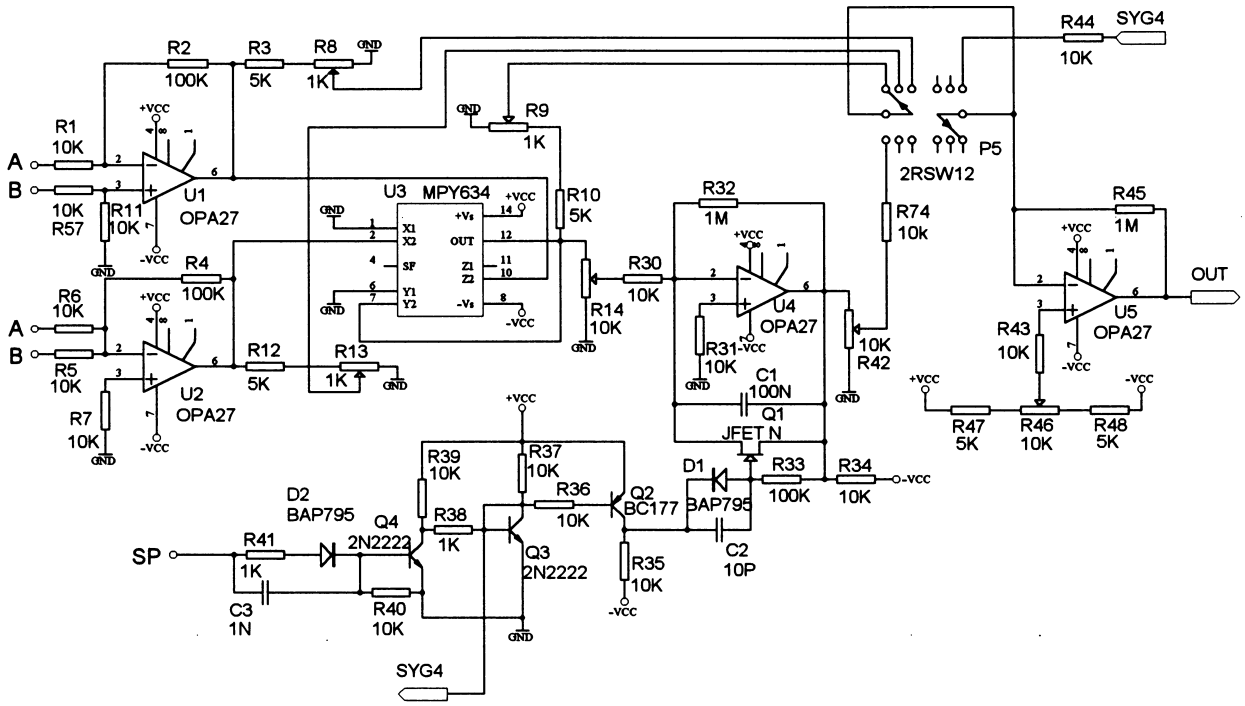

FIG. 14 Circuit diagram of the analogue processing system applied in MR-11.

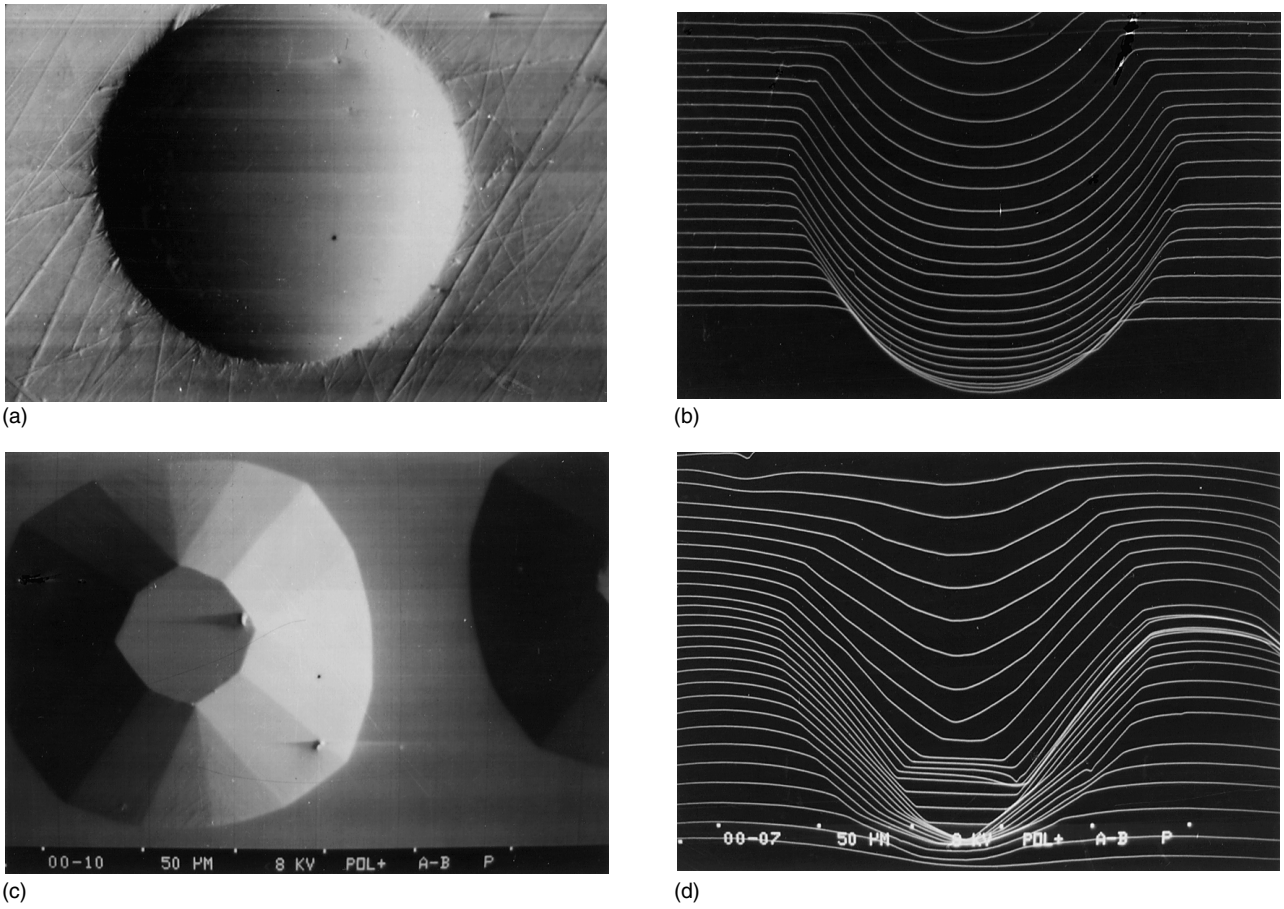

FIG. 15 Images for I_A–I_B signals and profiles obtained by means of the analogue processing system: (a,b) ball print in copper, r/h=1.67, horizontal field width = 750 μm; (c,d) etching in silicon, horizontal field width = 350 μm.

be advantageous for many other reasons. For instance, the beam range in solids decreases as the beam energy is reduced. Thus, the resolution limit connected with a finite size of the SE generation area may be improved at low energies. Of course, there is the usual problem of optimization because of the increasing beam diameter, but this deserves separate considerations. Anyway, the spatial resolution problem does not seem most crucial for many technological applications. For instance, profiles obtained by Tanaka *et al.* (1992) showed the resolution < 1 μm and 0.1 μm in lateral and vertical directions, respectively.

Conclusion

In this paper, a general model of the detector signal formation based on elementary relations concerning secondary electron emission has been presented. The signal modulation due to morphology and topography of the sample surface is defined here by simple analytical expressions. Also, the signal processing formula for surface profiling and its limitations results directly from the model. It should be stressed here that the method of a profile reconstruction can be applied as a rule only to continuous surfaces of slope angles < 90°. In practice, the maximum slope angles are limited by shadowing errors to much lower values. The error that matters most is that shadowing by the tangent plane and angles of shadowing by the topographic objects have to be greater than those of the former kind. As the sensitivity to topography as well as the limitations of shadowing errors depend directly on geometrical features of the detector system related to the object surface, the considerations presented may facilitate the design of a proper detection system for surface profiling. However, for objects of deeply modulated topography it should be a less sensitive system characterized by small detection and declination angles. In this case, noises will probably become a very important problem. On the other hand, a detection system of a great sensitivity and large detection and declination angles would be best for relatively smooth surfaces. Therefore, the most universal solution seems to be a system of two detectors enabling the change of its characteristic angles at will. We have taken steps to elaborate on such a detector system and hope to reveal first results in the near future.

References

Arnal F, Verdier P, Vincensini PD: Coefficient de rétrodiffusion dans de cas d'électrons monocinétiques arrivant sur la cible sous une incidence oblique. *Comp rend Acad Sci* (Paris) 268, 1526 (1969)

Czepkowski T: Reconstruction of surface profile in SEM using secondary electron signal. *Doctor thesis*. Wrocław (1994)

Czepkowski T, Słówko W: Reconstruction of surface topography in SEM. *Proc ICEM 13* Paris, 123–124 (1994)

Drzazga W, Grządziel I, Kubera C, Mokrauz I, Słówko W, Szymański H: Development of SEM with a two detector system. *Scanning* 9, 9–15 (1987)

Hasselbach F, Maier U: A few steps towards a more quantitative understanding of contrast in the scanning electron microscope. *Scan Microsc* 7, 21–32 (1993)

Hejna J: Detection of topographic contrast in the scanning electron microscope at low and medium resolution by different detectors and detector systems. *Scan Microsc* 8, 143–164 (1994)

Hejna J, Reimer L: Backscattered electron multidetector systems for improved quantitative topographic contrast. *Scanning* 9, 162–172 (1987)

Kanaya K, Kawakatsu H: Secondary electron emission due to plasmons and backscattered electrons. *J Phys D Appl Phys* 5, 1727–1742 (1972)

Kimoto S, Hasimoto H, Suganama T: Stereoscopic observation in scanning microscopy using multiple detectors. In *The Electron Microprobe* (Eds. McKinley TD *et al*.). John Wiley, New York (1966) 480–489

Lebiedzik J: An automatic topographical surface reconstruction in the SEM. *Scanning* 2, 230–237 (1979)

Reimer L: *Scanning Electron Microscopy*. Springer-Verlag (1985)

Reimer L, Riepenhausen M: Detector strategy for secondary and backscattered electrons using multiple detector systems. *Scanning* 7, 221–228 (1985)

Reimer L, Böngeler R, Desai V: Shape from shading using multiple detector signals in SEM. *Scan Microsc* 1/3, 963–973 (1987)

Schou J: Secondary electron emission from solids by electron and proton bombardment. *Scan Microsc* 3/2, 607–632 (1988)

Tanaka K, Nishimori K, Maeda K, Matsuda J, Hotta M: A scanning electron microscope with two secondary electron detectors and its application to the surface topography measurements of magnetic media. *Trans ASME* 114, 274–279 (1992)